Polymer 52 (2011) 1674–1685

Contents lists available at ScienceDirect

Polymer

journal homepage: www.elsevier.com/locate/polymer

Embedded metal nanoparticles as localized heat sources: An alternative processing approach for complex polymeric materials

Somsubhra Maity, Lori N. Downen, Jason R. Bochinski, Laura I. Clarke*

Department of Physics, NC State University, 2401 Stinson Drive, Box 8202, Raleigh, NC 27695-8202, USA

ARTICLE INFO

Article history:
Received 18 November 2010
Received in revised form
26 January 2011
Accepted 30 January 2011
Available online 25 February 2011

Keywords:
Nanocomposites
Surface plasmon resonance
Polymer processing

ABSTRACT

Metal nanoparticles were utilized as heating elements within nanofibers to demonstrate an alternative approach to thermally process nanostructured polymeric materials. In the photothermal process, resonant light excites the surface plasmon of the nanoparticle and the absorbed energy is converted into heat due to electron-phonon collisions. This heating is efficient and strongly localized, generated from the nanometer-sized metal particles embedded within the polymer. Composite polyethylene oxide (PEO) nanofibers, containing differing concentrations and types of nanoparticles, were fabricated by electrospinning and irradiated by a low intensity laser tuned specifically to the metal nanoparticle surface plasmon absorbance; aggregation of fibers, loss of fibrous structure, and ultimately, complete melting were observed. The photothermal response to irradiation increased with nanoparticle concentration as long as particle aggregation was avoided. Pure PEO nanofibers, or those containing metal nanoparticles possessing a non-resonant surface plasmon, were also irradiated but no melting occurred, demonstrating the controllable specificity of this approach.

1. Introduction

We discuss an alternative approach for selectively thermally treating polymeric materials—in particular, by demonstrating post-fabrication processing of electrospun nanofibrous mats. We observe that the photothermal effect of metal nanoparticles can be productively used in a polymeric nanostructured material environment for generating significant localized heating when the nanoparticles are contained within a polymer composite. Thus, the technique enables selective, in-situ thermal manipulation of polymers for repair or enhancement and the performance of processing tasks such as annealing, thermally-induced cross-linking, lamination, shape memory actuation, or specifically within nanofibrous mats, an improvement of fiber–fiber contacts without loss of the nanofibrous structure. Post-fabrication thermal processing of high porosity nanofibrous materials [1–5] is difficult due to the fragile and non-equilibrium physical properties of the samples [6], however we demonstrate that this photothermal approach directly allows such materials to be thermally controlled and manipulated at the nanoscale. In particular, metal nanoparticles acting as localized heaters are utilized to remotely process these materials using low laser intensity and without direct physical contact; the photothermal effect is highly selective, being dependent upon both the location of the particles and the wavelength of the excitation source (a property which can be tuned by altering the composition of the nanoparticles).

Metal nanoparticles exhibit a surface plasmon resonance [7–10] (SPR) due to the boundary conditions imposed on wave propagation by the limited spatial extent of the particle. The unique SPR frequency of a nanoparticle is influenced to differing degrees by its size, shape, composition, state of aggregation, and environment [11–20]. Optical excitation and non-radiative relaxation of the SPR of a nanoparticle creates a photothermal effect; that is, the conversion of light energy into heat. Within this SPR-mediated heating process, the light absorbed by the nanoparticle generates a non-equilibrium electron distribution that decays via electron–electron scattering. The hot electron gas equilibrates with lattice phonons which transfer this energy into the surrounding medium, resulting in a local temperature increase [10]. The total energy-transfer process is rapid (10^{-10}–10^{-12} s) and efficient [21]. While reports of SPR-mediated heating have appeared for some time [22–25], it has recently become apparent that this photothermal effect is a valuable nanoscale experimental tool [26–29] for a diversity of research initiatives such as controlled chemical release [30], vapor deposition [31–33], catalysis [34], and study of phase transitions [35]. However, few reports have addressed

* Corresponding author. Tel.: +1 919 513 7359; fax: +1 919 515 6538.
E-mail address: laura_clarke@ncsu.edu (L.I. Clarke).

0032-3861/$ – see front matter © 2011 Elsevier Ltd. All rights reserved.
doi:10.1016/j.polymer.2011.01.062

application of the photothermal effect in solid materials [12,36–41] and never in nanostructured polymer composites, or achieving such significant observable temperature changes while utilizing low incident light intensity.

Nanostructured polymeric materials such as electrospun composite nanofibrous mats are uniquely-suited to efficiently explore localized heating effects; such samples appear to the human eye as smooth film-like structures, however on the nanoscale are shown to consist of ~200 nm diameter cylindrical fibers randomly arranged in a low density collection [42]. In particular, electrospun nanofibrous materials which contain elongated polymer chains and large fractions of void space are intrinsically sensitive to even low levels of heating because it results in polymer and fiber-relaxation, fiber–fiber bonding, aggregation of fibers, and ultimately, melting; consequently, the energy provided by photothermal effect causes permanent physical alterations (i.e., significant morphological changes) which can be clearly observed and quantified even before a material phase change such as melting occurs. Moreover, when utilizing the SPR-mediated photothermal effect, the spatial extent and magnitude of the temperature change is highly dependent upon the thermal properties of the immediate environment surrounding the nanoparticle [27,36,43–45] and the overall system morphology. In these nanostructured samples, only a relatively small volume of material encompasses each nanoparticle (e.g., an 80 nm diameter spherical nanoparticle may reside within a ~200 nm diameter fiber surrounded predominantly by ~70% open space, with some overlapping points of fiber–fiber contacts). As a consequence of the large aspect ratio of the cylindrically-shaped fiber and the physical properties of the environment (e.g., the thermal conductivity for polyethylene oxide (PEO) at 28 °C [46] $k_{PEO} = 0.17$ W/mK and for the surrounding air $k_{air} = 0.024$ W/mK), the SPR-coupled energy diffuses away from nanoparticle (for the temperature ranges relevant here) conductively, propagating primarily along the fiber. Thus heat flow away from the nanoparticle is slow due to the small cross-sectional area of the fiber. In contrast, in a liquid medium heat loss occurs in all directions by both convection and conduction mechanisms. Furthermore, as the process is repeated for each photon absorbed by the nanoparticle, the slow loss of energy away from the particle results in a greater realizable local temperature increase in this nanostructured system even while utilizing low levels of light intensity. Hence, a significantly larger local temperature increase is generated for the same given energy input than would occur in a uniform, homogeneous environment with larger accessible material volumes and higher thermal losses (e.g., in an aqueous medium).

The advantages of efficient localized heating for processing, particularly of nanostructured materials, are immediately evident, especially if nanoparticles are strategically placed within a composite. Because the temperature change is primarily limited to the region surrounding the nanoparticles, selective placement of nanoparticles allows heating of particular sample regions without significantly affecting the remainder of the material. In addition, the photothermal effect enables heat to be generated from within a material, as opposed to conventional methods where the outer surface of the material is the first region to warm. Thus, processing at the nanoscale (nanoprocessing) can take place where heating is applied only to a preselected nanometer-sized region of the sample.

In contrast to the present report, the majority of previous work on the SPR-mediated photothermal effect using metal nanoparticles involved heating for biological or medical purposes [44,47–50], and therefore, these experiments utilized relatively spatially homogeneous, aqueous environments. In such water-based photothermal experiments, significantly higher light intensities ($\sim 10^5$ W/cm^2) must be used in order to generate the required thermal change than for the presently realized nanostructured polymer composites (~ 0.1 W/cm^2). For medical applications using metal nanoparticles, the approach normally involves short pulse, high intensity laser excitation at near infrared wavelengths which rapidly heats the surface of the particle and causes intentional shock heating of nearby cells for photothermal cancer therapy [50–53].

Electrospun nanofibrous mats, comprised of layers of nanometer-scale diameter fibers, are technologically-useful materials [42,54–57] due to their high surface area and relative ease of fabrication. Proposed uses for nanofibrous materials include biomedical [58–60] (tissue engineering, wound healing, drug delivery) as well as environmental (gas sensors, water purification, filtration) and energy [61] (fuel cells, solar cells) applications; accordingly, there has been much recent interest in developing methods for commercial scaling-up production of electrospun mats [62,63]. Furthermore, it is in principle straightforward to facilely create unique nanocomposite materials by doping the spinning solution with supplementary particles. Such additions are used to enhance the mechanical or electrical characteristics of the resultant nanofibers; however these embedded objects also have the (currently unrealized) potential to be utilized for in-situ post-processing and/or material repair via the photothermal effect.

In this report we demonstrate that the SPR-mediated photothermal effect can be usefully applied in non-aqueous environments, utilizing nanocomposite, nanofibrous mats to explore the capabilities offered by such remotely-controlled, spatially-selective heating in solid materials. For these polymeric materials, using the effect of localized heating may ultimately enable correction of defects from fabrication or damage from use (i.e., self-healing from cracks, crazes, or tears); increase fibrous mat mechanical strength while maintaining fiber morphology (i.e., from better fiber–fiber bonding); enable spatially-selective nanoprocessing (e.g., transforming portions of the material into film while leaving the remainder nanofibrous or selectively crystallizing the fiber interior while leaving the exterior amorphous); or novel nano-actuation (i.e., control of thermally-induced shape memory polymer materials via localized heating).

2. Experimental

2.1. Metal nanoparticles

Both gold and silver metal nanoparticles were utilized in this work. Two different gold nanoparticle forms were used; the first gold nanoparticle type (AuN_1) was spherical or slightly oblate citrate-stabilized particles that were fabricated in-house by utilizing the Frens' method [64]. Two batches using the identical procedure generated nanoparticles with different size distributions (batch #1: 80 ± 21 nm, batch #2: 29 ± 13 nm) which correspondingly displayed SPR extinctions peaks at 542 nm and 527 nm, respectively, as shown in Fig. 1 where transmission electron microscope (TEM) images of AuN_1 nanoparticles are provided as insets to the graphs of the normalized extinction measurements. The second gold nanoparticle type (AuN_2) was a commercially produced nanopowder colloid intercalated within an unknown polymer matrix and having a broadly specified size distribution of <100 nm. The silver nanoparticles (AgN) used were also a commercially available colloid formulation with a proprietary coating and a similarly specified distribution of <100 nm; subsequent TEM measurements determined an actual size distribution of 12 ± 5 nm.

The gold nanopowder colloid (636347-1G) (AuN_2), silver nanopowder colloid (576832-5G) (AgN), tetrachloroauric acid, sodium citrate, tetrahydrofuran (THF), and ethanol were obtained from Sigma–Aldrich. Polyethylene oxide (PEO) with molecular weight of 900,000 g/mol and analytical grade polyvinyl pyrrolidone (PVP) were supplied by Scientific Polymers Products Inc. All reagents were used without further purification.

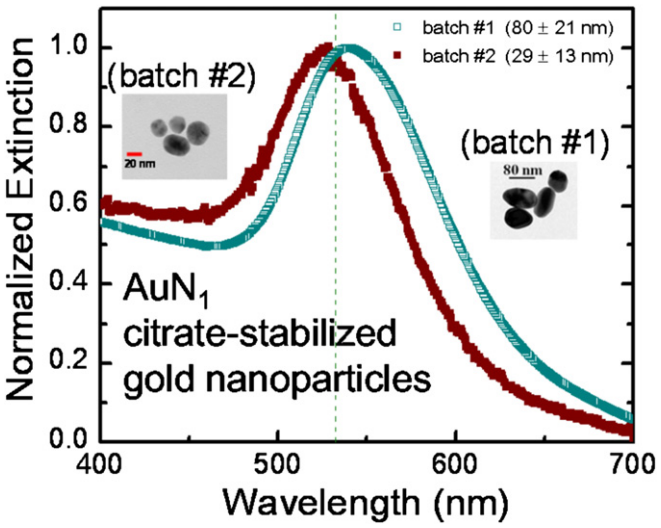

Fig. 1. Normalized extinction measurements for AuN_1 nanoparticles dispersed in water. Batch #1 has diameter size distribution 80 ± 21 nm and a SPR peak at 542 nm; batch #2 has diameter size distribution 29 ± 13 nm and a SPR peak at 527 nm. The vertical green line indicates the location of the 532 nm laser. The insets show TEM images of batch #1 and batch #2 AuN_1 nanoparticles. (For interpretation of the references to colour in this figure legend, the reader is referred to the web version of this article).

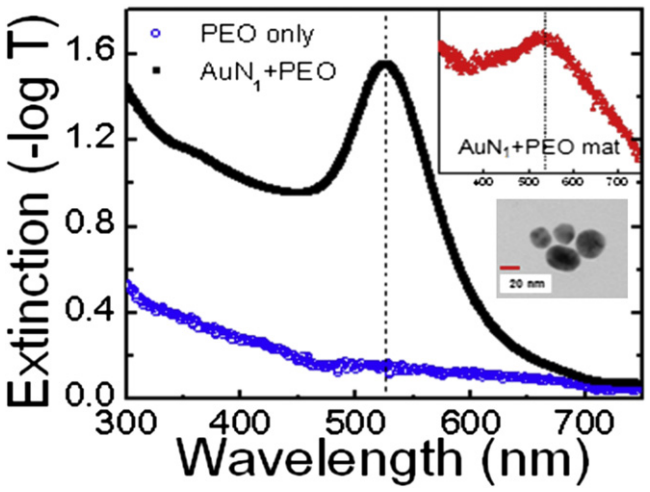

Fig. 3. Extinction measurements of PEO-only and AuN_1 + PEO spinning solutions. The solutions are diluted with water to ~0.25× of the actual electrospinning concentrations. The AuN_1 + PEO solution displays a peak at 527 nm indicated by a vertical dashed line. Inset: Extinction measurements of 5 stacked AuN_1 + PEO mats with peak at 538 nm indicated by a vertical dashed line. Lower image: TEM image of sample of AuN_1 nanoparticles with a 29 ± 12 nm diameter size distribution. AuN_1 nanoparticles (batch #2) are used for all of the measurements shown in the figure.

To fabricate the AuN_1 nanoparticles, aqueous tetrachloroauric(III) acid ($HAuCl_4$–$4H_2O$, 0.01 percent by weight (wt%)) was mixed with 300 mL tripled distilled water in a 500 mL round-bottom flask, and the solution was heated to boiling. The aqueous trisodium citrate (1.0 wt%, 10 mL) was injected quickly while the mixed solution kept boiling, and stirred for 10 min until the blue color suddenly changed to brilliant red, indicating nanoparticle formation. After cooling to room temperature, an amount of PVP equal to that of tetrachloroauric acid was immediately added to the solution to further stabilize the nanoparticles, prevent agglomeration, and act as a dispersing agent for the polymer solution. The citrate-stabilized nanoparticles (AuN_1) were spherical or slightly oblate, having a size distribution 80 ± 21 nm (batch #1) or 29 ± 13 nm (batch #2) in diameter.

2.2. Nanofibrous mat sample fabrication

4 wt% PEO solutions (PEO molecular weight 900,000 g/mol) in 2:1 water–ethanol mixtures by volume were utilized for electrospinning. For forming nanocomposite mats samples using AuN_1, dry polymer

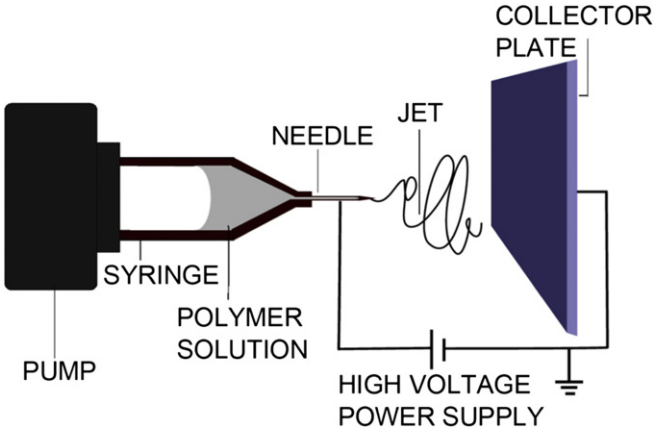

Fig. 2. Schematic of the traditional needle electrospinning apparatus for fabrication of nanostructured polymeric mats.

was added to a mixture of ethanol and the aqueous nanoparticle solution, resulting in a 2.5 wt% (nanoparticles–polymer) concentration. For the other gold (silver) particles used, dry powder of AuN_2 (AgN) was added to a pre-prepared PEO solution to obtain concentrations of 5 wt% and 25 wt% (25 wt%) nanoparticles, respectively. The stated concentration values are nanoparticle–PEO ratios in the final nanofiber formed after the solution has completely evaporated during the electrospinning process. The volume fraction is calculated by taking the ratio of the volume of nanoparticles to the sum of the volume of the nanoparticles and volume of PEO, using the known density of gold (19.3 g/cm^3) and PEO (1.13 g/cm^3 at 25 °C). Solutions with AuN_2 (AgN) were sonicated for 30 min to obtain a uniform suspension (solution) of nanoparticles. As a control sample, a solution of PEO-only was also identically prepared. All solutions were magnetically stirred for 1 h immediately prior to electrospinning.

Traditional needle electrospinning (Fig. 2) was performed in a horizontal orientation within a chemical fume hood. The apparatus consisted of a programmable syringe pump (New Era Pump Systems, Model NE 500) and a positive polarity, high voltage power supply (Glassman High Voltage, Model No. FC60R2). Polymer solutions (PEO-only, AuN_1 + PEO, AuN_2 + PEO, and AgN + PEO) were loaded into 10 mL syringes with a 4 inch 20 gauge blunt tip needle. The tip-to-collector distance was 25 cm, the voltage was 15 kV, and the pump was operated at a flow rate of 5 μL/min (8 μL/min) for PEO-only and AuN_1 + PEO (AuN_2 + PEO, AgN + PEO) solutions, respectively. Nanofibrous mats were collected after electrospinning for 40 min onto an aluminum foil sheet covering the flat, grounded collector plate. Mats were also directly electrospun onto open paper frames (creating unsupported, "free-hanging" samples), glass substrates, and metal stubs (used for scanning electron microscopy (SEM) imaging) for various diagnostic measurements. Nanofibers electrospun onto these collector surfaces display the same morphology and dimensions as those nanofibers spun onto the grounded aluminum foil.

2.3. Photothermal effect

A 100 mW, 532 nm (25 mW, 405 nm) continuous-wave diode laser was expanded to approximately uniformly illuminate a ~1 cm^2 area

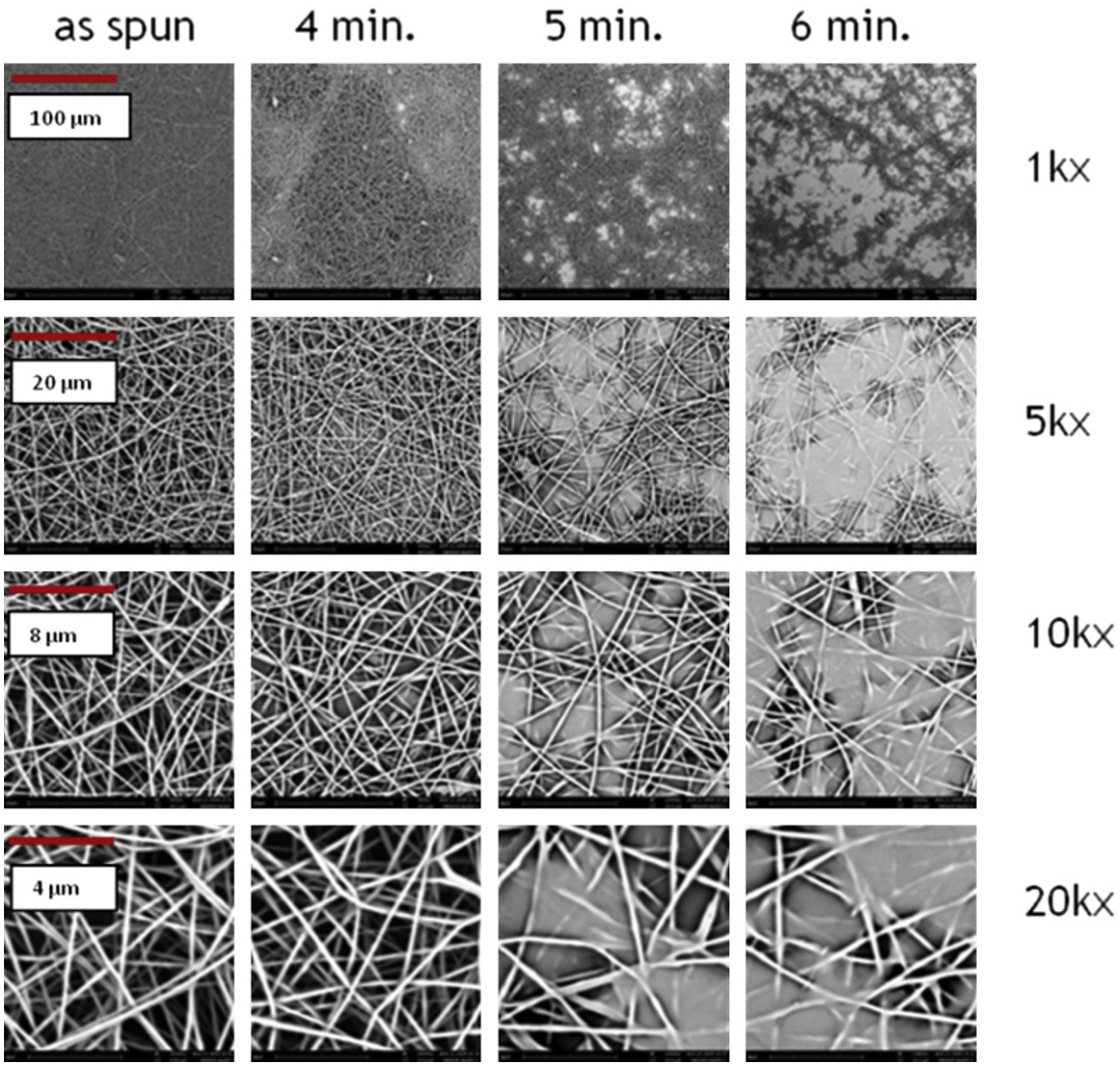

Fig. 4. SEM images of the effect of continuous 532 nm light irradiation on AuN_1 + PEO nanofibrous mats (0.15% volume fraction AuN_1 batch #1). Column labels (top, right to left) indicate increasing irradiation times in minutes; row labels (right side, top to bottom) indicate increasing magnification levels (e.g., 1000 times = 1k×). After 4 min (2nd column), fiber aggregation is observed. After ≥5 min (3rd and 4th columns), the fibers exhibit melting and film-like regions are formed; note that intact fibers are still present alongside the melted regions. For the longest time displayed (6 min irradiation, 4th column), the majority of the mat area has melted.

of the sample mat for specified periods of time to excite the SPR of the gold (silver) nanoparticles with an intensity of ~0.1 W/cm^2 (~0.025 W/cm^2).

2.4. Sample characterization

Extinction spectra of electrospinning solutions diluted with water to 0.25× of the actual spinning solution or the subsequently formed nanofibrous mats were measured with an ultraviolet–visible spectrometer (CARY 50 Scan) to identify the location of the SPR.

Nanofibrous mats were characterized via comparison of scanning electron microscopy (SEM) images taken before and after irradiation. To decrease charging, ~10 nm of Au/Pd was sputtered coated onto the samples before imaging. All images were obtained by SEM (FEI Phenom-World BV) and analyzed using the ImageJ software. The linear measurement tool of the program determined the diameter of selected nanofibers, with the average and standard deviation values of ~20 separate data points reported. The mat porosity was calculated by identifying the relative area of void spaces in the 10kx images for a single layer of the mat [65–67].

The TEM images were obtained using a Hitachi HF2000 Transmission Electron Microscope. PEO spinning solution doped with nanoparticles was electrospun onto copper grids coated with a 400 nm thick carbon layer having 2 μm holes and 2 μm spacing (Protochips CF-2/2-2C-25) to investigate the fiber sizes and the distribution of nanoparticles within the fibers. For determining the size distribution of the different available metal nanoparticles, nanoparticle solutions were drop-cast directly onto the grids.

3. Results and discussion

3.1. Nanocomposite mats with gold nanoparticles

Nanofibrous mats of PEO fibers doped with citrate-stabilized gold nanoparticles (AuN_1) were electrospun. The nanoparticles were fabricated in-house using the Frens' method [64]. Due to the chemical compatibility of the stabilizing shell, AuN_1 particles readily disperse in the water–ethanol solvent system used for the PEO electrospinning solutions, however the particle concentration is relatively low, and cannot be easily increased. The SPR for well-dispersed spherical gold particles in solution depends on particle

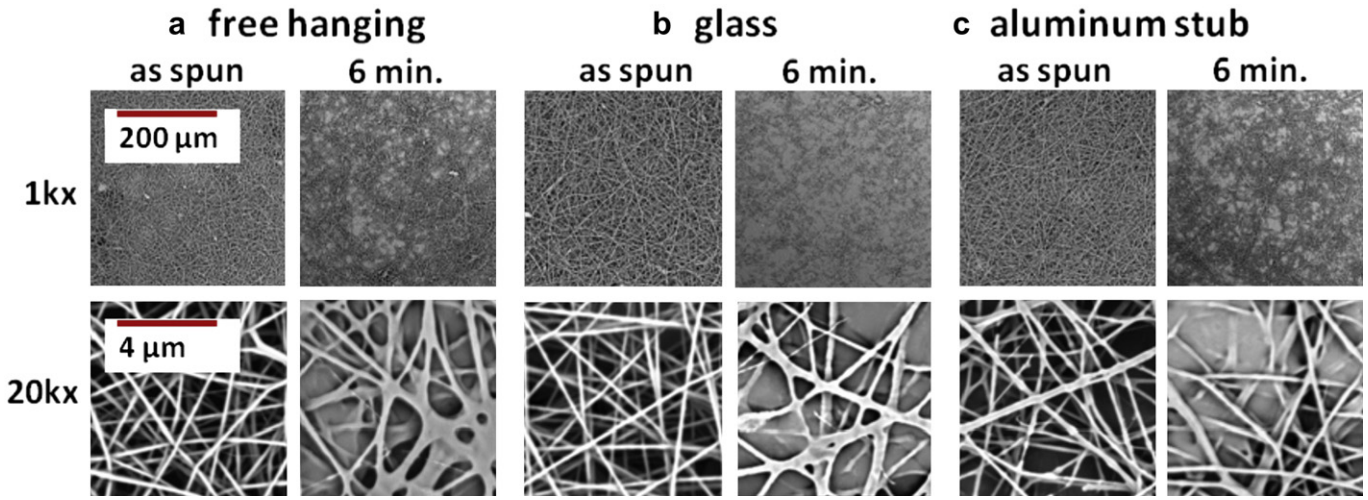

Fig. 5. Photothermal effect for $AuN_1 + PEO$ mats electrospun onto different substrates. Left side column shows "as spun" mat (1st, 3rd, and 5th columns); right side column after 6 min of irradiation by the 0.1 W/cm^2 532 nm laser (2nd, 4th, and 6th columns). a) Unsupported mat ("free-hanging"), b) glass slide, and c) aluminum stub (used for SEM imaging) all display fiber melting. The direction of laser illumination of the samples were a) from the top viewed surface down through the mat; b) and c) from the back side of the sample through the front (top) surface.

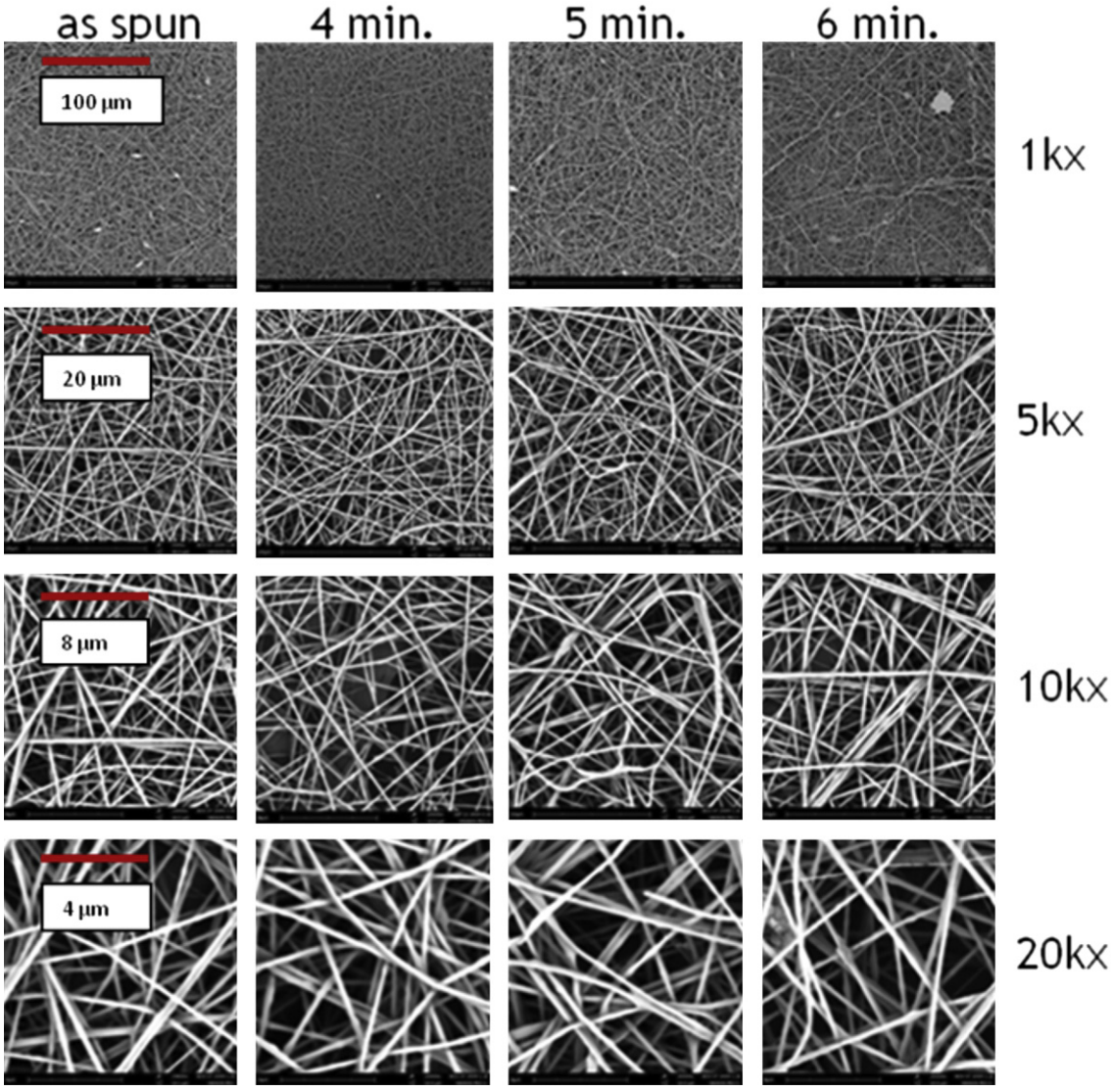

Fig. 6. SEM images of PEO-only nanofibers. The light intensity and irradiation times are identical to those in Fig. 4. No fiber melting is observed.

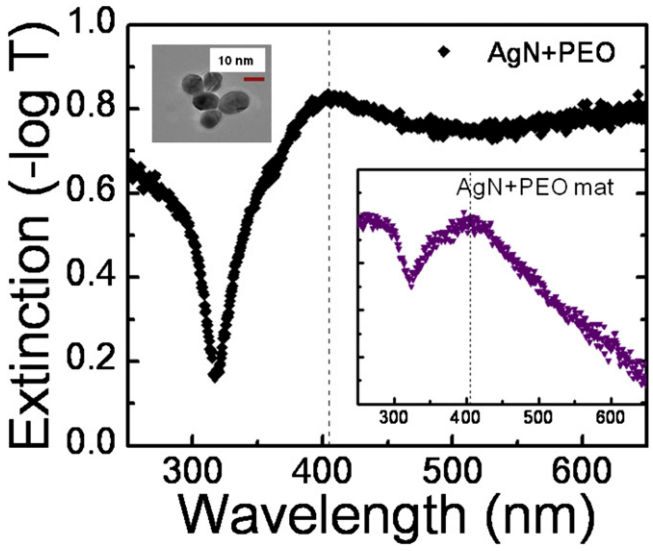

Fig. 7. Extinction measurement of AgN + PEO spinning solution, diluted to 0.25× with water from actual electrospinning concentration. The AgN + PEO solution displays a peak at 405 nm indicated by a vertical dashed line. Inset: Extinction measurements for a single AgN + PEO mat with peak at 405 nm indicated by a vertical dashed line. Upper image: TEM image of sample of isolated AgN nanoparticles with a 12 ± 5 nm diameter size distribution.

size and shifts slightly toward longer wavelengths for larger diameter nanoparticles [11,16,23]. Two formulations of AuN_1 nanoparticles with different size distributions (batch #1: 80 ± 21 nm; batch #2: 29 ± 13 nm) were used in the experiments, displaying SPR extinctions peaks at 542 nm and 527 nm, respectively, as previously shown in Fig. 1. Fig. 3 depicts extinction measurements for pure PEO and AuN_1 + PEO spinning solutions (using AuN_1 batch #2 nanoparticles), as well as the subsequently electrospun nanocomposite AuN_1 + PEO mat (upper inset). The extinction is defined as the negative of the logarithm of the transmittance T. The spectral location of the SPR peak for AuN_1 gold nanoparticles in water or in the PEO solvent spinning solution remains essentially unchanged; in the solid environment of the electrospun mat, it undergoes a small shift. In contrast, the PEO spinning solution does not present any spectrally-distinct extinction peak. The lower inset in Fig. 3 (also shown in Fig. 1) depicts a TEM image of the AuN_1 batch #2 particles.

Fig. 4 shows a series of scanning electron microscope (SEM) images demonstrating the effect of irradiating PEO nanofibrous mats containing a dilute concentration of AuN_1 particles (AuN_1 batch #1 at 0.15% volume fraction) with 532 nm laser light with an intensity of ~0.1 W/cm^2. The mats are initially composed of nanofibers with diameters 232 ± 41 nm. Mat samples are typically a few microns in thickness; the depth of field of the SEM image brings the top few layers of nanofibers into focus. For reference, the bulk melting temperature of PEO is approximately 65–70 °C [68]. As shown in Fig. 3, the SPR of the AuN_1 nanoparticles in the mat may shift spectral location slightly but still remains highly resonant with the fixed frequency irradiation laser. The four columns represent separate samples taken from the same electrospun mat exposed to the laser for different times. From the upper to the lower level, the four rows display increasing magnification of the images, indicated on the right side (e.g., 1000× = 1k×). For comparison, the leftmost column (1st column, "as spun") presents mat sample images without laser irradiation. As seen clearly (Fig. 4, 3rd column "5 min" and 4th column "6 min"), even at the relatively low light intensity levels and dilute gold nanoparticle doping levels used, after a few minutes of irradiation sufficient heat is generated to significantly melt the PEO nanofibers. The melted regions appear as whitish, featureless regions in the images. After 4 min of continuous irradiation, the primary effect is fiber aggregation (light streaks in the 1k× image). At 5 min, film-like regions (i.e., the much lighter areas) are observed within the sample superimposed on intact or aggregated fibers; after 6 min, the majority of the mat displays some film-like morphology and most intact fibers show aggregation or melting and merging into other fibers.

The heating/melting originates from random locations across the mat and then expands, eventually (at the longest irradiation time shown) encompassing the majority of the sample. Within the images, the heating/melting is initially extremely localized as intact fibers are present alongside the melted, film-like regions. These results have been reproduced with free hanging or substrate-supported mats, on transparent or opaque substrates, and with mats spun from different PEO solutions; always the same effects are observed and thus the influence of the supporting substrate (if any) on the demonstrated heating process is minimal. Fig. 5 depicts SEM images of AuN_1 + PEO mats which are either free hanging or supported by different solid substrates displaying similar heating from the photothermal effect.

3.2. Mats without metal nanoparticles

Results for experiments performed on pure PEO mats are shown in Fig. 6. The electrospun mats were subjected to identical irradiation parameters as those in Fig. 4; however, the PEO-only nanofibers do not contain any metal nanoparticles. The mats are initially comprised of distinct nanofibers having diameters 229 ± 55 nm, which remain intact. As seen in the figure, no melting or fiber aggregation (which would be suggestive of low-level heating) is observed in any of the images, which is also consistent with the lack of a distinct extinction peak for the PEO. This result demonstrates that significant heating only occurs in the presence of the nanoparticles via the photothermal effect.

We note that the small film-like regions (e.g., light features in 1k×, "as spun" image; or upper right structure in 1k×, "6 min" image) are not from heating but due to infrequent electrospraying events which occurred during the initial mat fabrication when a small solution droplet was ejected onto the collector plate and dissolved pre-existing nanofibers. Moreover, the only detrimental side-effect of the irradiation (affecting an extremely small portion of the sample) that was observed after examining all the images of the mats (not shown) composed of PEO-only was occasional fiber-relaxation and a few cases of fiber-breakage. This may be an indication of a very weak, non-specific light-PEO interaction. In electrospun nanofibers, polymer chains are often aligned along the fiber axis; upon relaxation, fibers curl dramatically, which can lead to ruptures at weak points in the fiber.

3.3. Nanocomposite mats with silver nanoparticles

Another set of experiments were performed by forming composite PEO fibers using a commercial silver colloid nanopowder (AgN). The AgN particles have proprietary organic coating (to aid in dispersing the particles in polar solvents) and an unknown size distribution, broadly specified by the manufacturer as "<100 nm". As the AgN particles readily solvate when stirred in the water–ethanol spinning solutions, using the powder form enables the nanoparticle concentration to be easily varied at will. Silver nanoparticles possess a plasmon absorption peak near 400 nm, far detuned from the SPR frequency for spherical gold particles (>520 nm) and the green irradiation laser wavelength of 532 nm. Extinction measurements for the spinning solution of AgN + PEO in a water–ethanol mixture (Fig. 7) confirm the

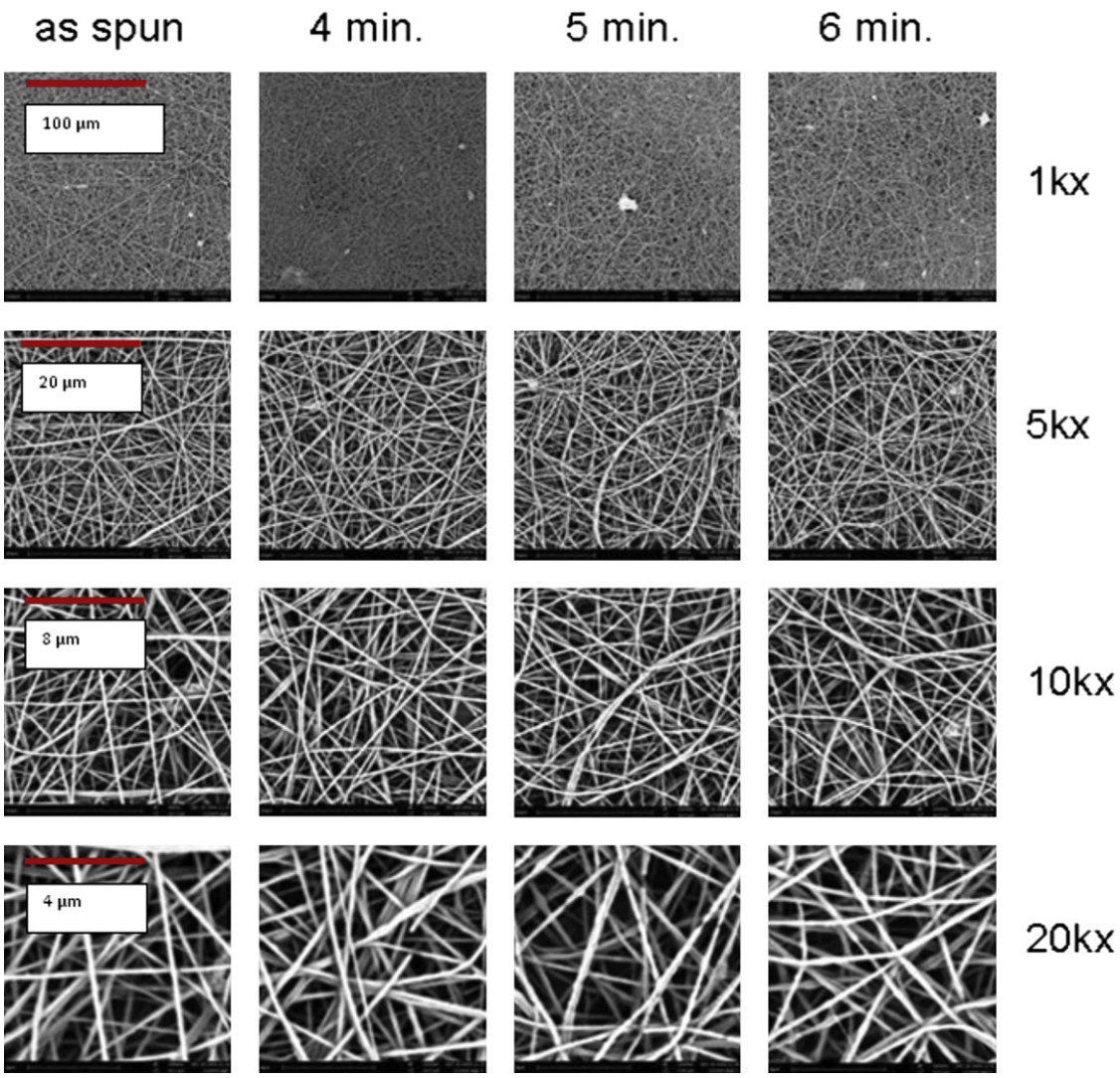

Fig. 8. SEM images of PEO nanofibers doped with 1.5% volume fraction silver nanoparticles (AgN + PEO). The light intensity and irradiation times are identical to those used for Figs. 2 and 3. No fiber melting is observed when the samples are irradiated with the 532 nm laser.

presence of an absorbance peak around 405 nm. The minimum in the spectra that occurs around ~320 nm is a consequence of the intrinsic dielectric constant of silver [20,69]. Electrospun mats of silver nanoparticle–doped PEO (1.5% volume fraction of AgN) were composed of nanofibers with diameters 232 ± 43 nm. The lower graph inset in Fig. 7 reveals that the spectral location of the SPR of the AgN within the mat environment remains unchanged from the spinning solution. An example TEM image of AgN particles is shown in the upper left of the figure; analysis of a series of such images indicate the AgN particles in the experiment possess a diameter size distribution of 12 ± 5 nm.

The results of irradiation of the AgN + PEO nanofibrous mats with the 532 nm green laser are shown in Fig. 8. As with the PEO-only nanofibers, under these illumination conditions the AgN + PEO nanofibers exhibit a small amount of fiber-relaxation and some minor fiber-breakages, but no melting. Hence, it is clearly necessary for the irradiating light source and SPR of the particular metal nanoparticle used to be matched in order to generate heating via the photothermal effect. Consequently, since the silver nanoparticles do possess a SPR located at ~405 nm, when the PEO mats doped with AgN are irradiated with light resonant with the silver nanoparticles' SPR, subsequent melting of the mats should logically be expected.

Fig. 9 shows the SEM images of the effect of irradiation of the AgN + PEO mats with an approximately uniformly-expanded, 405 nm continuous-wave laser at an intensity of ~0.025 W/cm^2. While the photothermal effect for silver nanoparticles should provide greater heating per photon absorbed (by ~1.3×) because the SPR is lower in wavelength then for gold nanoparticles, the time period of irradiation until observed melting of the sample is extended relative to the AuN_1 + PEO mats in Fig. 4 because the violet laser (405 nm) intensity was proportionally weaker than the green laser (532 nm). For these irradiation conditions, the onset of fiber melting takes place around 10 min; by the end of 20 min of continuous irradiation, a majority of the fibers have melted.

3.4. Photothermal effect for selective processing

The fact that the heating of the polymer nanocomposite via the photothermal effect is dependent on the SPR frequency of the doped metal nanoparticles can be utilized in developing nano-processing techniques of considerable specificity. The SPR of nanoparticles composed of different metals are sufficiently separated in frequency and the available laser systems are suitably spectrally-narrow that, in a sample comprised of multiple

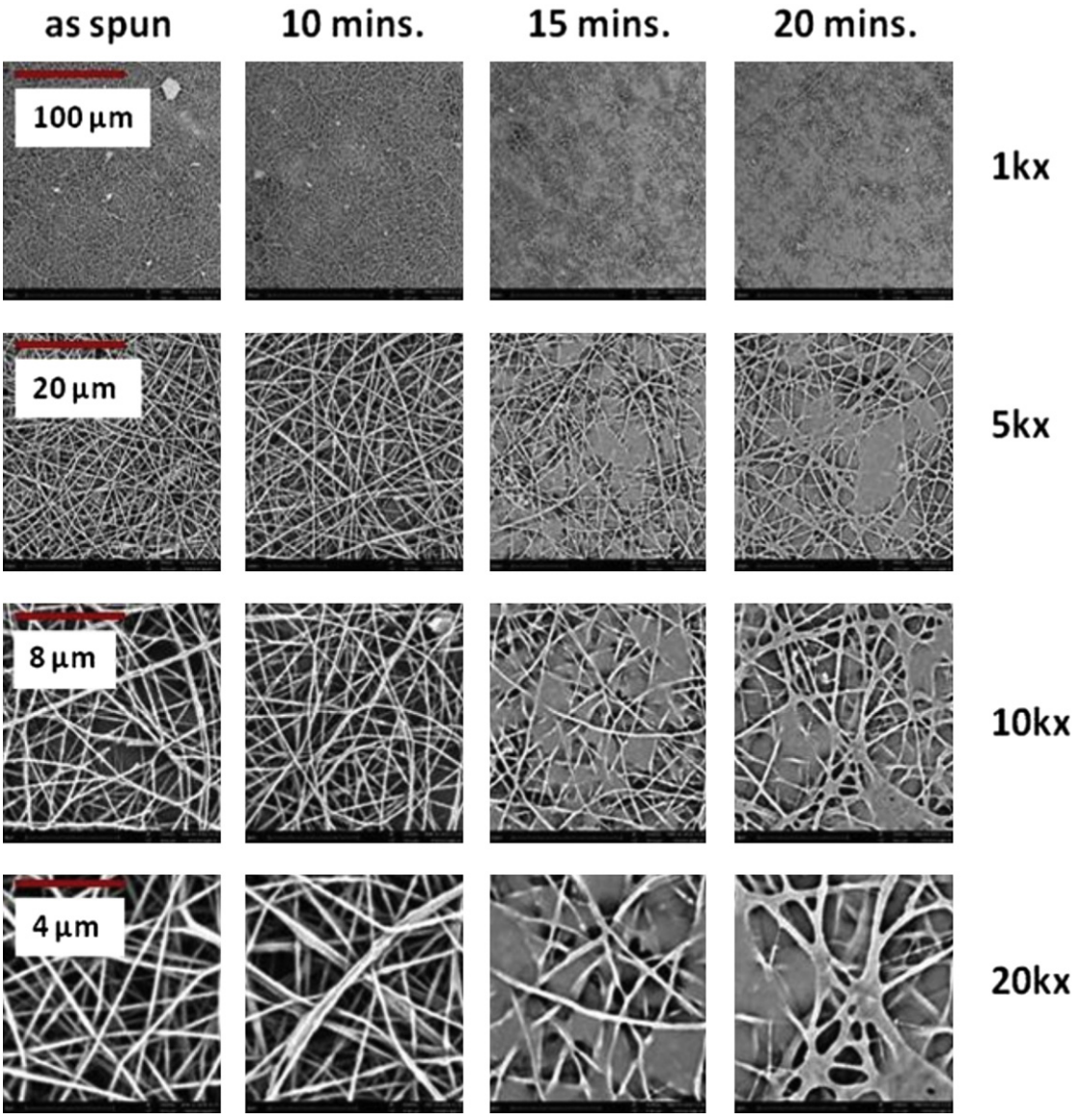

Fig. 9. SEM images of the effect of continuous 405 nm light irradiation on AgN + PEO nanofibrous mats (1.5% volume fraction AgN). After 10 min (2nd column), fiber aggregation is observed. After ≥15 min (3rd and 4th columns), the fibers exhibit melting and film-like regions are formed; note that fibers are still present alongside the melted regions. For the longest time displayed (20 min irradiation, 4th column), the majority of the mat area has melted.

nanostructured components with different metal nanoparticles, one could chose which structure to heat by using the corresponding laser while leaving the other structures unaffected. This could occur in overlapping nanofibers possessing different doped particles; in composite coaxial electrospun samples where either the inner core or outer sheath portions of the fibers could be facilely targeted; or nanostructured features composed of metal nanoparticles blended into shape memory materials, which upon heating, undergo phase change and alter their morphology.

Effectively utilizing the photothermal energy conversion process to generate a quantifiable temperature change ΔT in a medium relative to the environment relies on optimizing the exchange between the deposition of energy into the system Q_{in} and the loss of energy from the system Q_{out}. The basic factors that determine Q_{in} are 1) the nanoparticle concentration; 2) several parameters associated with suitably coupling the light field to the SPR of the nanoparticle: the intrinsic size, shape, and composition of the nanoparticle, the laser frequency, and possible small spectral shifts induced by the presence of the medium; 3) the laser intensity; and 4) the total length of time of the irradiation (until a steady-state balance is achieved). The Q_{out} from the system is controlled by the inter-related factors of 1) the thermal coupling between the medium and the environment; 2) the material properties of the medium/environment; and 3) the morphology of the medium/environment. Under steady-state conditions, energy flowing out can be expressed [16,21] as $Q_{out} = (h)(A)(\Delta T)$, where h is the thermal transfer coefficient and A is the cross-sectional area for the conduction; in this case, it is most useful to assume that the heat transfer from the nanoparticle to the surrounding polymer is efficient and apply this formula to a small segment of polymeric nanofiber containing a nanoparticle, where ΔT is the increase in temperature of the polymer relative to the environment. While h is difficult to estimate [16] because of the nanostructure of the system and the surrounding environment (i.e., void space), the energy loss is dominated by conduction along the nanofibers and A becomes the cross-sectional area of the fiber. In contrast, embedding the particle within a spatially uniform medium allows heat loss in all directions, without the transport "bottleneck" of a small cross-

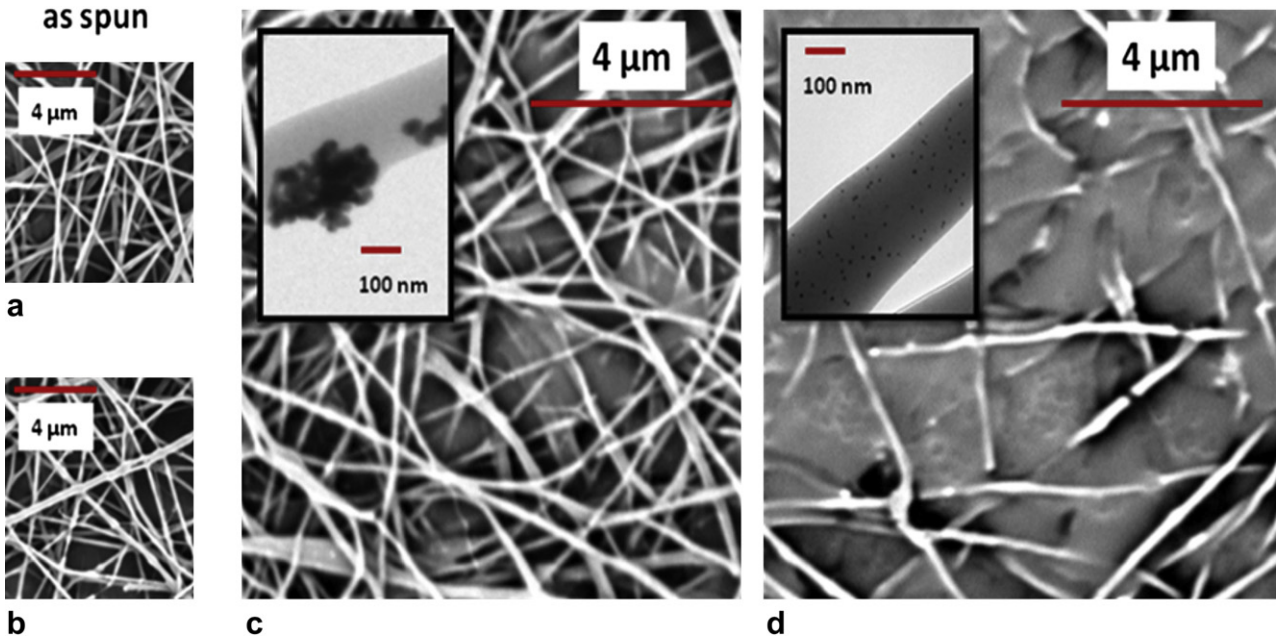

Fig. 10. SEM image of AgN + PEO nanofibers as initially fabricated when the silver nanoparticles are (a) agglomerated, or (b) well-dispersed. SEM images of the samples after identical laser irradiation time for mats with the (c) agglomerated and (d) well-dispersed AgN particles. Inset: TEM images of the nanofibers, showing the distribution of the AgN particles within the fibers.

sectional area in the thermally-isolated (i.e., by the void space) nanofiber. Normally, in utilizing the photothermal effect, researchers have focused their attention on optimizing Q_{in} by selecting the laser frequency to match the SPR of their particular nanoparticle and increasing the laser intensity. In the present work, we introduce a paradigm shift in thinking by not only suitably coupling the light field to the SPR but, instead of increasing the irradiating photon flux, have enhanced the heating by also altering Q_{out}. In particular, the use of nanostructured polymeric materials with void spaces is an effective tailoring of the sample and the environment to optimize localized heating by decreasing Q_{out}—restricting efficient heat transfer from the nanoparticle only along the fiber. Thus, embedding the localized heat sources within the nanosized polymeric structures which are shaped to have small cross-sectional areas relative to their lengths (i.e., a large aspect ratio) surrounding by void space regions essentially condenses the deposited energy to create a maximal thermal effect.

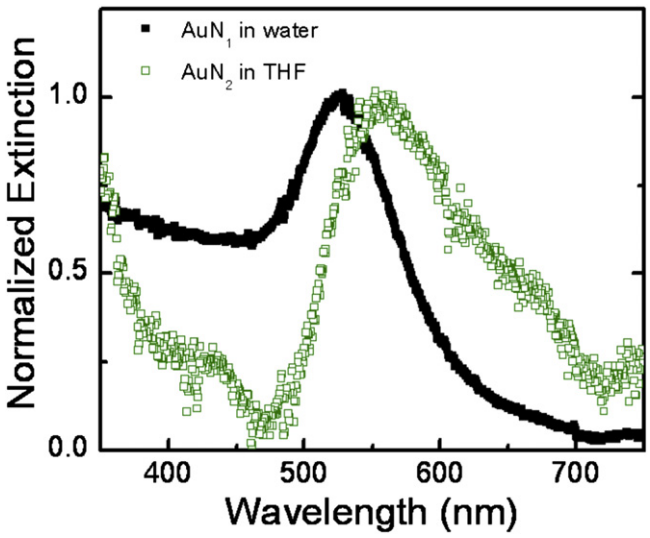

Fig. 11. Normalized extinction measurements comparing AuN_1 in water and AuN_2 in THF. The AuN_1 (batch #2) particles are well-dispersed with an SPR at 527 nm and a diameter distribution of 29 ± 13 nm. The AuN_2 particles are slightly dispersed in the THF solvent but also form agglomerations of larger clusters, giving rise to the broadening of the SPR peak to the longer wavelengths.

As suggested above, one logical route toward further enhancing the measurable temperature change ΔT resulting from the photothermal effect of embedded metal nanoparticles within a medium is increasing the particle concentration. For well-separated nanoparticles, additional nanoscale heat sources will proportionally add to the thermal energy deposited in the system [21,41,43] (i.e., linearly increasing Q_{in}). In principle, the nanoparticle concentration can be raised continuously until the approximation of isolated nanoparticles is no longer valid and collective particle effects due to particle–particle interactions must be considered [17,18]. This limitation occurs when the particle-to-particle separation $d < 5r$, where r = radius of the particle [16]. Under such conditions, the consequence on the photothermal conversion process is complicated, dependent upon the precise cluster structure and its orientation relative to the polarization direction of the irradiating light field [27]. In general, the primary effect of increasing the density of nanoparticles and forming larger clusters (i.e., agglomeration) is a spectral shift in the SPR of the ensuing structure toward longer wavelengths relative to that of the isolated nanoparticles [17,18]. Such a situation can also occur under conditions when, though the average concentration of particles is extremely dilute, agglomeration of nanoparticles leads to formation of cluster structures and a detrimentally high local density. In the context of the present report, such a circumstance of increased average concentration (with unintended agglomeration of particles) might paradoxically lead to reduction in the efficiency of the photothermal effect as particle density is increased, as the SPR of the clusters is more detuned relative to the fixed frequency of the irradiating laser.

3.5. Experimental effect of nanoparticle agglomeration

Nanoparticle agglomeration is a troublesome, but common experimental complication in composite systems. The chemical

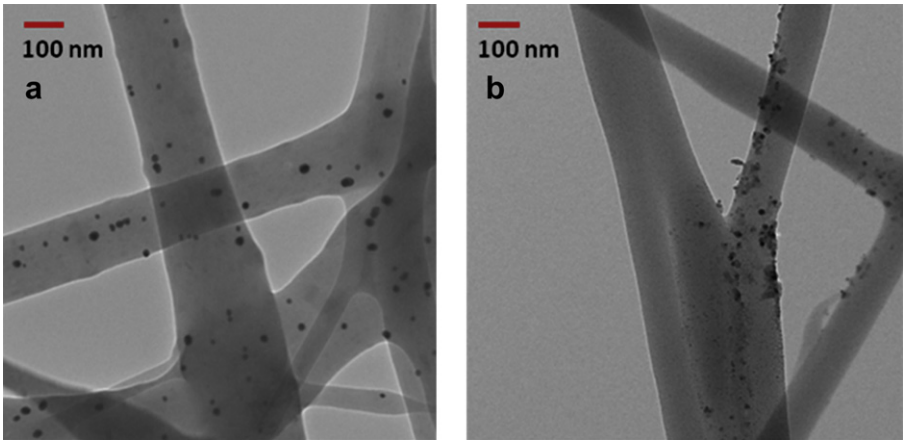

Fig. 12. TEM images reveal the differences in effectiveness in dispersing the two types of gold nanoparticles. a) AuN_1 nanoparticles are well-separated within the nanofibers. b) AuN_2 nanoparticles tend to be agglomerated within the PEO nanofibers.

composition of a nanoparticle shell is nominally selected to facilely enhance solubility of the particle within the chosen environment and normally prevents detrimental particle–particle interaction. For instance, the proprietary coating on the commercial silver nanoparticles (AgN) effectively enables the particles to solvate in the water–ethanol spinning solutions when well-agitated. However, when a poorly-stirred sample of the AgN + PEO solution was electrospun, some nanoparticles were subsequently clumped together within the fibers (inset TEM image Fig. 10c is an example of such agglomeration of particles). In contrast, fibers formed from a sample solution which was agitated sufficiently prior to electrospinning exhibited a homogeneous distribution of nanoparticles within the fibers (inset TEM image Fig. 10d shows well-separated nanoparticles). Such aggregation has no obvious detrimental effect on the ability to electrospun either solution and demonstrably produces high quality nanofibers (SEM images of the "as spun" fibers in Fig. 10a and b are essentially identical). However, Fig. 10 further illustrates how the difference in particle distribution

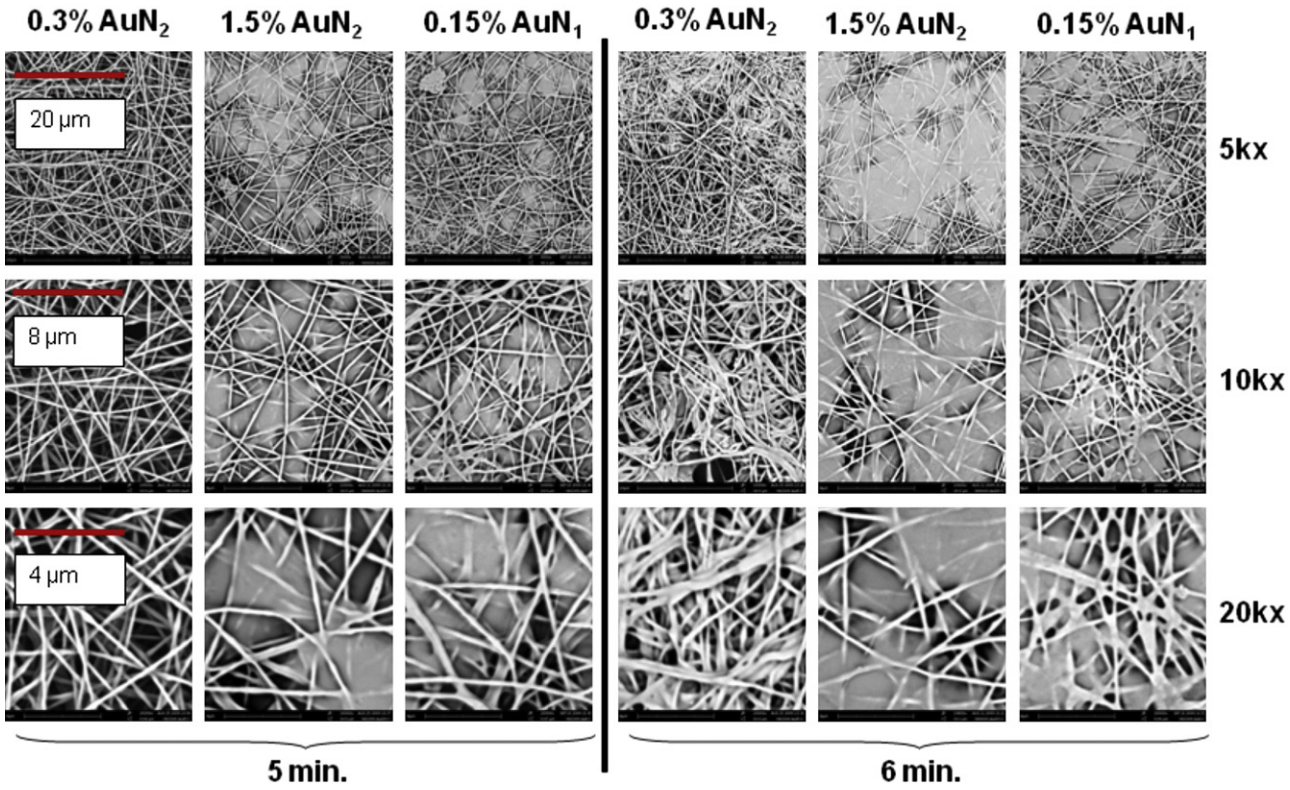

Fig. 13. Comparison of different nanoparticle types and concentrations on the localized heating effect within the mats. For AuN_2 + PEO mats at 0.3% volume fraction of particles, no effects from heating are noticeable after 5 min of irradiation (1st column); however, at 6 min, fiber aggregation is observed, indicating a softening and relaxation of the nanofibers (4th column). Increasing the nanoparticle content by 5× results in the production of melted fibers at 5 min (2nd column), with the sample becoming almost completely film-like after 6 min of irradiation (5th column). Because the AuN_1 particles remain well-dispersed and do not agglomerate into larger clusters with spectrally-shifted SPRs, a lower doping level (0.15% volume fraction for AuN_1 + PEO mats) produces similar results of heating (3rd, 6th columns) to the 1.5% volume fraction doping level for mats containing the AuN_2 particles (2nd, 5th columns). The mats are all irradiated using the same 0.1 W/cm^2, 532 nm laser.

within the fibers impacts the ability to melt the nanofibrous mats via the photothermal effect. When both samples are irradiated identically (0.025 W/cm^2 for 15 min with a 405 nm continuous-wave laser), the fibers with well-dispersed AgN particles exhibit significantly more melting (Fig. 10d) than those containing the aggregated particles (Fig. 10c). We note that some heating of the AgN + PEO nanofibers formed with clumped nanoparticles still does occur, because not all the AgN particles in the sample are agglomerated, but the overall heating effect is noticeably diminished.

In order to further study the effect of nanoparticle doping level and agglomeration, we compared the efficacy of the photothermal effect using a commercial gold nanopowder colloid (AuN_2), which possesses distributed particle sizes <100 nm and an unknown polymer matrix, to our homemade gold citrate-stabilized nanoparticles (AuN_1, batch #1 80 ± 21 nm). In principle, by utilizing the nanopowder colloid, the nanoparticle concentration can be facilely varied; however, in practice, we observed that the commercial AuN_2 particles did not solvate in the water–ethanol solution and formed suspensions. In contrast, the homemade nanoparticles (AuN_1) are citrate-stabilized, readily solvated in the spinning solution, and form a homogenous, well-separated mixture. Despite considerable efforts using common solvents, heating, sonication, and stirring for extensive amounts of time, the commercial gold nanopowder remained resilient toward going into solution; ultimately, the AuN_2 particles were discovered to weakly solvate in tetrahydrofuran (THF) after stirring for several days. Fig. 11 shows comparison of normalized extinction measurements for AuN_1 (batch #2) particles in water and AuN_2 particles in THF. The AuN_2 in THF spectrum displays a noticeable broadening toward longer wavelengths, indicative of the formation of large clusters with a distribution of sizes. It is expected that within the water–ethanol spinning solution the aggregation effect is even more prevalent and thus should be similarly present within the electrospun mats. This condition has been confirmed by observing the TEM images of PEO nanofibers doped with the two types of nanoparticles, clearly demonstrating the AuN_2 particles are aggregated together, whereas AuN_1 particles are dispersed within the fibers (Fig. 12). We note that there is no preferred cluster size formed by the agglomeration therefore it is likely a wide range of cluster sizes are present, that a small subset of well-separated individual particles is also probably present, and that within the mat sample there is no organized alignment of the clusters with respect to the irradiation field.

Subsequently, due to these aggregation effects which shift the plasmon resonance to the longer wavelengths, a considerable fraction of the AuN_2 nanoparticles are expected to have limited responsiveness to the irradiation laser. The consequence of this cluster-formation is that a higher volume fraction of AuN_2 will be required in order to generate the same level of heating (under the same intensity of irradiation), as depending on the extent of the SPR-shift for the clusters, they may still interact with the irradiation light, albeit far less efficiently, and only some small undetermined fraction of the particles will remain separated and act as efficient local light-driven heaters.

The SPR-mediated heating results for 0.3% and 1.5% volume fraction AuN_2 samples are directly compared with 0.15% volume fraction AuN_1 doped mats in Fig. 13 and confirm this prediction. The 0.15% volume fraction AuN_1 samples show the greatest photothermal effect and exhibit resultant heating which is similar to mats comprised of an order of magnitude higher concentration 1.5% volume fraction AuN_2. The 0.3% volume fraction AuN_2 sample exhibits a smaller response than the other two samples, reflecting the presence of fewer heat sources (i.e., intrinsic SPR and irradiation source wavelength not as well matched) in the nanofibrous sample interior.

As detailed in Fig. 13, the lower concentration AuN_2 + PEO mat (0.3% volume fraction, 1st column) displayed few effects due to heating after 5 min of irradiation, whereas mats possessing five times higher concentration (1.5% volume fraction, 2nd column) or at a lower doping of the more photo-thermally active homemade nanoparticle (AuN_1 + PEO 0.15% volume fraction, 3rd column) show widespread fiber melting. After 6 min of continuous laser excitation, these trends continue with some apparent melting now observed in the more dilute sample of the commercial nanoparticle (4th column) and virtually total melting of the other mat samples (5th and 6th columns), respectively.

4. Conclusions

These results unequivocally demonstrate that SPR-mediated heating can be utilized to heat, melt, and otherwise alter nanofibrous materials from the interior. Remarkably, due to the nanofibrous morphology and properties of the nanostructured polymer sample and environment, significant photothermal heating can occur using low intensity, continuous-wave visible laser irradiation. Moreover, it is clear that the heating initiates at extremely localized spatial locations and is selectively controllable due to the specificity provided by the metal nanoparticle SPR. Increasing the concentration of nanoparticles can proportionally increase the degree of thermal effects, as long as conditions leading to aggregation of the nanoparticles are avoided.

Acknowledgments

This work was supported by NSF CMMI-0829379 and the Faculty Research and Professional Development Fund at NC State University. We would like to thank Dr. Keith Weninger (NCSU Physics) for use of equipment, Dr. Joseph Tracy (NCSU Material Science and Engineering) for support with nanoparticle preparation, and Dr. Russell Gorga (NCSU Textile Engineering, Chemistry, and Science) for technical advice.

References

[1] Dai TH, Yu H, Zhang K, Zhu MF, Chen YM, Adler HJ. Journal of Applied Polymer Science 2008;107(4):2142–9.
[2] Lee SJ, Oh SH, Liu J, Soker S, Atala A, Yoo JJ. Biomaterials 2008;29(10):1422–30.
[3] Wei KY, Vigo TL, Goswami BC. Journal of Applied Polymer Science 1985;30(4):1523–34.
[4] You Y, Lee SW, Lee SJ, Park WH. Materials Letters 2006;60(11):1331–3.
[5] Zong XH, Ran SF, Fang DF, Hsiao BS, Chu B. Polymer 2003;44(17):4959–67.
[6] Tan EPS, Lim CT. Composites Science and Technology 2006;66(9):1102–11.
[7] Bohren CF, Huffman DR. Absorption and scattering of light by small particles. New York: Wiley; 1983.
[8] Kreibig U, Vollmer M. Optical properties of metal clusters. Berlin: Springer-Verlag; 1995.
[9] Daniel MC, Astruc D. Chemical Reviews 2004;104(1):293–346.
[10] Maier SA, Atwater HA. Journal of Applied Physics 2005;98(1):10.
[11] Jain PK, Lee KS, El-Sayed IH, El-Sayed MA. Journal of Physical Chemistry B 2006;110(14):7238–48.
[12] Harris N, Ford MJ, Cortie MB. Journal of Physical Chemistry B 2006;110(22):10701–7.
[13] Muskens OL, Billaud P, Broyer M, Fatti N, Vallee F. Physical Review B 2008;78(20):9.
[14] Muskens OL, Del Fatti N, Vallee F, Huntzinger JR, Billaud P, Broyer M. Applied Physics Letters 2006;88(6):3.
[15] Zhao J, Pinchuk AO, McMahon JM, Li SZ, Ausman LK, Atkinson AL, et al. Accounts of Chemical Research 2008;41(12):1710–20.
[16] Cortie MB, Xu X, Chowdhury H, Zareie H, Smith G. In: Said FA-S, editor. Plasmonic heating of gold nanoparticles and its exploitation, vol. 5649. SPIE; 2005. p. 565–73.
[17] Liz-Marzan LM. Langmuir 2006;22(1):32–41.
[18] Ung T, Liz-Marzan LM, Mulvaney P. Colloids and Surfaces. A, Physicochemical and Engineering Aspects 2002;202(2–3):119–26.
[19] Westcott SL, Oldenburg SJ, Lee TR, Halas NJ. Chemical Physics Letters 1999;300(5–6):651–5.

[20] Kelly KL, Coronado E, Zhao LL, Schatz GC. Journal of Physical Chemistry B 2003;107(3):668–77.
[21] Richardson HH, Carlson MT, Tandler PJ, Hernandez P, Govorov AO. Nano Letters 2009;9(3):1139–46.
[22] Del Fatti N, Flytzanis C, Vallee F. Applied Physics B-Lasers and Optics 1999;68 (3):433–7.
[23] Link S, El-Sayed MA. Journal of Physical Chemistry B 1999;103(40):8410–26.
[24] Berciaud S, Lasne D, Blab GA, Cognet L, Lounis B. Physical Review B 2006;73 (4):8.
[25] Boyer D, Tamarat P, Maali A, Lounis B, Orrit M. Science 2002;297 (5584):1160–3.
[26] Baffou G, Quidant R, Girard C. Applied Physics Letters 2009;94(15):3.
[27] Govorov AO, Richardson HH. Nano Today 2007;2(1):30–8.
[28] Baffou G, Quidant R, de Abajo FJG. ACS Nano 2010;4(2):709–16.
[29] Baffou G, Kreuzer MP, Kulzer F, Quidant R. Optics Express 2009;17(5):3291–8.
[30] Skirtach AG, Dejugnat C, Braun D, Susha AS, Rogach AL, Parak WJ, et al. Nano Letters 2005;5(7):1371–7.
[31] Boyd DA, Greengard L, Brongersma M, El-Naggar MY, Goodwin DG. Nano Letters 2006;6(11):2592–7.
[32] Cao LY, Barsic DN, Guichard AR, Brongersma ML. Nano Letters 2007;7 (11):3523–7.
[33] Hung WH, Hsu IK, Bushmaker A, Kumar R, Theiss J, Cronin SB. Nano Letters 2008;8(10):3278–82.
[34] Adleman JR, Boyd DA, Goodwin DG, Psaltis D. Nano Letters 2009;9 (12):4417–23.
[35] Urban AS, Fedoruk M, Horton MR, Radler J, Stefani FD, Feldmann J. Nano Letters 2009;9(8):2903–8.
[36] Mohamed MB, Ahmadi TS, Link S, Braun M, El-Sayed MA. Chemical Physics Letters 2001;343(1–2):55–63.
[37] Bhargava A, Cortie MB. Journal of Nanophotonics 2007;1:13.
[38] Alessandri I, Depero LE. Nanotechnology 2008;19(30):7.
[39] Chen H, Liu X, Muthuraman H, Zou JH, Wang JH, Dai Q, et al. Advanced Materials 2006;18(21):2876.
[40] Cortie MB, Harris N, Ford M. Physica B-Condensed Matter 2007;394 (2):188–92.
[41] Richardson HH, Thomas AC, Carlson MT, Kordesch ME, Govorov AO. Journal of Electronic Materials 2007;36(12):1587–93.
[42] Burger C, Hsiao BS, Chu B. Annual Review of Materials Research 2006;36:333–68.
[43] Govorov AO, Zhang W, Skeini T, Richardson H, Lee J, Kotov NA. Nanoscale Research Letters 2006;1(1):84–90.
[44] Hu M, Chen JY, Li ZY, Au L, Hartland GV, Li XD, et al. Chemical Society Reviews 2006;35(11):1084–94.
[45] Zeng N, Murphy AB. Nanotechnology 2009;20(37):8.
[46] Song L, Chen YF, Evans JW. Journal of the Electrochemical Society 1997;144 (11):3797–800.
[47] Jain PK, El-Sayed IH, El-Sayed MA. Nano Today 2007;2(1):18–29.
[48] Jain PK, Huang XH, El-Sayed IH, El-Sayed MA. Accounts of Chemical Research 2008;41(12):1578–86.
[49] Huang XH, Jain PK, El-Sayed IH, El-Sayed MA. Lasers in Medical Science 2008;23(3):217–28.
[50] Huff TB, Tong L, Zhao Y, Hansen MN, Cheng JX, Wei A. Nanomedicine 2007;2 (1):125–32.
[51] Day ES, Morton JG, West JL. Journal of Biomechanical Engineering-Transactions of the ASME 2009;131(7):5.
[52] Nedyalkov NN, Imamova SE, Atanasov PA, Toshkova RA, Gardeva EG, Yossifova LS, et al. Comptes Rendus De L Academie Bulgare Des Sciences 2010;63(5):767–74.
[53] Wang ST, Chen KJ, Wu TH, Wang H, Lin WY, Ohashi M, et al. Angewandte Chemie-International Edition 2010;49(22):3777–81.
[54] Huang ZM, Zhang YZ, Kotaki M, Ramakrishna S. Composites Science and Technology 2003;63(15):2223–53.
[55] Tan S, Huang X, Wu B. Polymer International 2007;56(11):1330–9.
[56] Reneker DH, Yarin AL, Zussman E, Xu H. Electrospinning of nanofibers from polymer solutions and melts. In: Advances in applied mechanics, Vol. 41. San Diego: Elsevier Academic Press Inc; 2007. 43–195.
[57] McCullen SD, Ramaswamy S, Clarke LI, Gorga RE. Wiley Interdisciplinary Review: Nanomedicine and Nanobiotechnology 2009;1:369.
[58] Liang D, Hsiao BS, Chu B. Advanced Drug Delivery Reviews 2007;59 (14):1392–412.
[59] Nair LS, Bhattacharyya S, Laurencin CT. Expert Opinion on Biological Therapy 2004;4(5):659–68.
[60] Pham QP, Sharma U, Mikos AG. Tissue Engineering 2006;12(5):1197–211.
[61] Thavasi V, Singh G, Ramakrishna S. Energy & Environmental Science 2008;1 (2):205–21.
[62] Zhou FL, Gong RH, Porat I. Polymer International 2009;58(4):331–42.
[63] Muthuraman NT, Bochinski JR, Clarke LI, Gorga RE. Polymer 2010;51:4928.
[64] Frens G. Nature-Physical Science 1973;241(105):20–2.
[65] McCullen SD, Stevens DR, Roberts WA, Ojha SS, Clarke LI, Gorga RE. Macromolecules 2007;40(4):997–1003.
[66] Ojha SS, Stevens DR, Hoffman TJ, Stano K, Klossner R, Scott MC, et al. Biomacromolecules 2008;9(9):2523–9.
[67] Ojha SS, Stevens DR, Stano K, Hoffman T, Clarke LI, Gorga RE. Macromolecules 2008;41(7):2509–13.
[68] Wang W, Bushby AJ, Barber AH. Applied Physics Letters 2008;93(20):3.
[69] Ma YW, Wu ZW, Zhang LH, Zhang J. Chinese Physics Letters 2010;27(2):4.